Article:
Fa, R and Zhang, L (2013) Generalised grouped minimum mean-squared errorbased multi-stage interference cancellation scheme for orthogonal frequency division multiple access uplink systems with carrier frequency offsets. IET Communications, 7 (7). pp. 685-695. ISSN: 1751-8628

https://doi.org/10.1049/iet-com.2012.0285

Generalized Grouped MMSE Based Multi-stage Interference Cancellation Scheme for OFDMA Uplink Systems with CFOs

Rui Fa [†] and Li Zhang [‡]

Abstract

In uplink OFDMA systems with CFOs, there always be a dilemma that high performance and low complexity can not be obtained simultaneously. In this paper, in order to achieve better trade-off between performance and complexity, we propose a grouped minimum mean squared error (G-MMSE) based multi-stage interference cancellation (MIC) scheme. The first stage of the proposed scheme is a G-MMSE detector, where the signal is detected group by group using banks of partial MMSE filters. The signal group can be either user based or subcarrier based. Multiple novel IC units are serially concatenated with the G-MMSE detector. Reusing the filters in the G-MMSE detector significantly reduces the computational complexity in the subsequent IC units as shown by the complexity analysis. The performance of the proposed G-MMSE-MIC schemes are evaluated by theoretical analysis and simulation. The results show that the proposed schemes outperform other existing schemes with considerably low complexity.

Index Terms – Orthogonal frequency division multiple-access (OFDMA), interference cancellation (IC), multiuser interference (MUI), carrier frequency offset (CFO).

I. Introduction

Orthogonal frequency division multiple access (OFDMA) has recently attracted a great deal of research interest due to its potential of high spectral efficiency, inherent immunity to multipath

[†]Dr. Rui Fa is with the University of Liverpool, Liverpool, Email: r.fa@liverpool.ac.uk;

[‡] Dr. Li Zhang is with School of Electronic and Electrical Engineering, University of Leeds, Leeds, LS2 9JT, United Kingdom. l.x.zhang@leeds.ac.uk.

This work is supported by the UK Engineering and Physical Sciences Research Council (EPSRC).

fading and simplified equalization [1]–[11]. It has been selected as one of the physical-layer multiple-access technologies in the recent wireless metropolitan area network (MAN) standard IEEE 802.16 [12] and 3GPP-LTE [13]. Despite its appealing features, OFDMA is extremely sensitive to carrier frequency offsets (CFOs), which may be induced by Doppler effects and/or a misaligned local oscillator. The presence of CFOs results in the loss of mutual orthogonality among subcarriers, produces both intercarrier interference (ICI) and multiuser interference (MUI), and degrades the system performance [8], [9]. Counteracting CFOs in OFDMA uplink is particularly difficult mainly due to two reasons. Firstly, CFO estimation is a difficult job in uplink OFDMA, apparently due to the presence of multiple CFOs [3], [8], [14], [15]. Secondly, the detection is also challenging even given perfect CFO estimation, because the compensation of one user's CFO would misalign other users and cause severe MUI [5], [9]–[11], [16]–[19]. It is a common practice to employ a particular synchronization policy where the CFOs are estimated during the downlink phase, then returned by a downlink control channel and compensated at each user before uplink transmission [20]. However, even with this approach, residual frequency errors may be present in the received uplink signals at the base station (BS) due to estimation errors and/or Doppler shifts. In this case, novel synchronization and compensation algorithms are still required at the BS [7], [10].

In this paper, we focus on the compensation assuming that CFO estimation has been accomplished [14], [15]. There are a few schemes proposed for detection in uplink OFDMA systems with CFOs. In [16], the CLJL scheme (named after the four authors' initials) was proposed to compensate the CFOs after the discrete Fourier transform (DFT) using circular convolution rather than before the DFT. Apart from the CLJL scheme, other schemes can be roughly grouped into two categories: one is for interference cancellation (IC) schemes including parallel interference cancellation (PIC) using circular convolution, such as Huang-Letaief Circular Convolution (HLCC) [10] and weighted linear PIC (WLPIC) [11] schemes, and also including selective PIC (SPIC) [9] and successive interference cancellation (SIC) schemes [17]; the other is for minimum mean squared error (MMSE) based schemes [5], [18], [19]. On one hand, ~~most of~~ the above IC schemes, namely, CLJL, HLCC, WLPIC, cannot provide satisfactory performance when the normalized CFOs (by subcarrier spacing) are greater than 0.3 (or less than -0.3), while the range of the normalized CFOs $[-0.5, 0.5)$ is more reasonable [18]. On the other hand, MMSE-based schemes are too complex to implement due to the requirement of matrix inversion.

Although [18], [19] proposed banded method and iterative implementation to approach MMSE scheme, the computational complexity is still high. Moreover, both IC schemes and MMSE-based schemes degrade much with the generalized carrier assignment scheme (GCAS), which is the current trend in OFDMA due to its flexibility for dynamical resource allocation [7], [10].

In this paper, we propose a grouped minimum mean squared error (G-MMSE) based multi-stage interference cancellation (MIC) scheme for the uplink OFDMA systems with CFOs, in order to achieve better trade-off between performance and complexity. Although group-wise interference cancellation (GIC) has been discussed in the CDMA and MIMO systems [21], [22], there are many questions to be answered when applying the group-wise IC concept in the uplink OFDMA systems with CFOs, for example, how to form a group, how to cancel interference and what is the theoretical performance. The GIC schemes for CDMA and MIMO systems are similar, as a MIMO spatial multiplexing system can be equivalently viewed as a CDMA system. The code signatures (CDMA) or the spatial signatures (MIMO) are broken into many small groups while in OFDMA systems, there is no such signature. Thus, the GIC scheme has to be tailored according to the specifications of the OFDMA system. To our best knowledge, there is no contribution to the group-wise IC for the uplink OFDMA systems in the literature so far. Here, we propose a scheme which consists of multiple stages. The first stage is a G-MMSE detector, where the signal is detected group by group using banks of partial MMSE filters. The grouping can be user-based and subcarrier-based. Multiple novel IC units, which are different with the conventional SIC and PIC schemes, are serially concatenated with the G-MMSE detector. Because the filters in the G-MMSE detector can be reused in the subsequent IC units, the computational complexity is greatly reduced according to the complexity analysis. Furthermore, the bit error probability (BEP) performance of the proposed scheme is theoretically analysed and validated by simulations. The numerical results show that the proposed G-MMSE-MIC schemes outperform other existing schemes with considerable low complexity.

The main contributions we have made in our paper are listed as follows

1) A G-MMSE detector is proposed. Both user-grouped (UG) and subcarrier-grouped (SCG) methods are described and investigated for the OFDMA uplink system.
2) An IC unit, which is different with the conventional SIC and PIC schemes, is proposed.
3) Multiple IC units are serially concatenated with the G-MMSE detector. The computational complexity is greatly reduced since the filters in the G-MMSE detector can be reused in

the subsequent IC units.

4) The complexity analysis and theoretical BEP performance analysis are carried out.

The rest of paper is organized as follows. Sec. II presents the uplink OFDMA system model. The G-MMSE algorithm is developed for the uplink OFDMA systems and the UG and SCG methods are presented in Sec. III. Sec. IV describes the proposed IC units and MIC scheme. Subsequently, Sec. V carries out the complexity analysis and theoretical performance analysis. Finally, the simulation results and conclusions are given in Sec. VI and VII, respectively.

II. System Model For OFDMA Uplink

The OFDMA uplink system under consideration consists of one base station (BS) and K user terminals communicating with the BS simultaneously. For simplicity, we assume that both time synchronization and sampling are ideally performed as [10] did. Reader who are interested in the algorithms achieving time synchronization may refer to [8] and references therein. Suppose that N subcarriers are used for transmitting signal and are evenly divided into K' ($K' \geq K$) subchannels. To avoid aliasing problem at the receiver, a number N_0 of null subcarriers are placed at both edges of the signal spectrum. Each subchannel contains $N_c = (N - 2N_0)/K'$ subcarriers. Denoting the i-th block of frequency-domain modulated symbols sent by the k-th user as $\boldsymbol{s}_k(i)$, where $k \in \{1, 2, ..., K\}$, and the j-th entry of $\boldsymbol{s}_k(i)$ is non-zero only if the j-th subcarrier is assigned to the k-th user. Define a mapping vector $\boldsymbol{\mathcal{M}}_k = \{\mathcal{M}_k^j | j = 1, ..., N\}$ to indicate the subcarrier mapping for the k-th user, where the subcarrier assignment is given by

$$\mathcal{M}_k^j = \begin{cases} 1 & j \text{ is assigned to the } k\text{-th user} \\ 0 & j \text{ is not assigned to the } k\text{-th user} \end{cases}. \tag{1}$$

We also define an index vector $\boldsymbol{\mathcal{I}}_k$ with the length of N_c to record the indices of subcarriers assigned to the k-th user. For the subband carrier assignment scheme (SCAS), the subcarriers assigned to one user are adjacent while for the GCAS, they are assigned in a random fashion. A cyclic prefix (CP) of length N_p is appended to eliminate the inter-block interference (IBI). The resulting signal $\boldsymbol{u}_k(i)$ with the length of $N + N_p$ is transmitted over the channel. The multipath channel, which is a tapped delay line (TDL) model, is assumed static over an OFDM block but it may vary from block to block. Let $\boldsymbol{h}_k(i) = [h_k^0(i), h_k^1(i), ..., h_k^{N_h-1}(i)]^T$ denote the discrete-time channel impulse response (CIR) of the k-th user during the i-th block, where $(\cdot)^T$ is the transpose

operator and N_h is the channel length, which is usually less than or equal to $(N_p + 1)$. Without loss of generality, we drop the block index i in the following text for simple notation. After serial-to-parallel (S/P) conversion and the CP removal, an N dimensional vector $\boldsymbol{y}$ is formed. Let ϵ_k denote the CFO normalized by subcarrier spacing between the k-th user and the BS, which is uniformly distributed over the range of $[-0.5, 0.5)$. The received OFDMA signal vector $\boldsymbol{y}$ in the presence of CFOs is mathematically written as

$$\boldsymbol{y} = \sum_{k=1}^{K} \boldsymbol{\Gamma}(\epsilon_k)\boldsymbol{\mathcal{H}}_k \boldsymbol{F}^H \boldsymbol{s}_k + \boldsymbol{n}, \tag{2}$$

where

- $\boldsymbol{\Gamma}(\epsilon_k) = \text{diag}(1, e^{j2\pi\epsilon_k/N}, ..., e^{j2\pi\epsilon_k(N-1)/N})$;
- $\boldsymbol{F}$ is the N-point discrete Fourier transform (DFT) matrix with entries $\boldsymbol{F}_{p,q} = \frac{1}{\sqrt{N}} \exp\left(\frac{-j2\pi pq}{N}\right)$, $(0 \leq p, q \leq N-1)$ and $(\cdot)^H$ denotes the Hermitian transpose;
- $\boldsymbol{\mathcal{H}}_k$ is the circulant channel convolution matrix corresponding to the k-th user;
- $\boldsymbol{n}$ is circularly symmetric white Gaussian noise with zero-mean and covariance matrix $\sigma_n^2 \boldsymbol{I}_N$, where $\boldsymbol{I}_N$ is the identity matrix of order N and σ_n^2 is the noise power.

According to [23], we note that $\boldsymbol{\mathcal{H}}_k = \boldsymbol{F}^H \mathcal{D}(\boldsymbol{H}_k)\boldsymbol{F}$, where $\mathcal{D}(\cdot)$ is diagonal matrix operator and $\boldsymbol{H}_k$ is the channel frequency response (CFR), which is obtained by $\bar{\boldsymbol{F}}\boldsymbol{h}_k$, where $\bar{\boldsymbol{F}}$ is the first N_h columns of $\boldsymbol{F}$.

After applying DFT on (2), the frequency-domain received signal vector $\boldsymbol{Y}$ can be written as

$$\begin{aligned} \boldsymbol{Y} &= \sum_{k=1}^{K} \boldsymbol{F}\boldsymbol{\Gamma}(\epsilon_k)\boldsymbol{F}^H \mathcal{D}(\boldsymbol{H}_k)\boldsymbol{s}_k + \boldsymbol{F}\boldsymbol{n}, \\ &= \boldsymbol{\Pi}\boldsymbol{s} + \boldsymbol{v}, \end{aligned} \tag{3}$$

where

- $\boldsymbol{\Pi} = \sum_{k=1}^{K} \boldsymbol{F}\boldsymbol{\Gamma}(\epsilon_k)\boldsymbol{F}^H \mathcal{D}(\boldsymbol{H}_k)\mathcal{D}(\boldsymbol{\mathcal{M}}_k)$;
- $\boldsymbol{s} = \sum_{k=1}^{K} \boldsymbol{s}_k$;
- $\boldsymbol{v} = \boldsymbol{F}\boldsymbol{n}$ is the frequency-domain noise vector.

III. Grouped MMSE Algorithm

In this section, the grouped MMSE (G-MMSE) algorithm for OFDMA uplink systems is presented. Using the full MMSE (FMMSE) algorithm proposed in [18], the detected soft symbol

$\boldsymbol{z}_f$ is given by

$$\boldsymbol{z}_f = \boldsymbol{W}_f^H \boldsymbol{Y}, \tag{4}$$

where

$$\boldsymbol{W}_f = \left(\boldsymbol{\Pi}\boldsymbol{\Pi}^H + \frac{\sigma_n^2}{\sigma_s^2} \boldsymbol{I}_N \right)^{-1} \boldsymbol{\Pi}, \tag{5}$$

where subscript f denotes the FMMSE scheme and σ_s^2 is the averaged power of the transmitted signal on one subcarrier. The detected soft symbols $\boldsymbol{z}_f$ finally can be demodulated to bit streams. Due to the operation of matrix inversion, the FMMSE algorithm is too complex for practical use, especially when the system size is large. For this reason, [18], [19] proposed banded method and iterative implementation to approach FMMSE scheme, however, their computational complexity is still high. In this paper, we propose a low-complexity G-MMSE algorithm, which detects the signal group by group using banks of small size filters. Note that the G-MMSE is not a true MMSE filter but a simplified MMSE or partial MMSE filter. Considering the truth that the most impactive MAI comes from the neighbouring subcarriers, the G-MMSE scheme ignores part of MAI by employing small size filters to achieve a trade-off between performance and complexity. The signal can be grouped according to either associated users, termed as user-grouped (UG) method or adjacent subcarriers termed as subcarrier-grouped (SCG). In the subsequent subsections, we will introduce them in details, respectively.

A. User-Grouped Method

In the UG method, we organize the subcarriers allocated to the same user into one group, and apply MMSE. Thus, the detection of the k-th user is mathematically given by

$$\begin{aligned} \boldsymbol{z}_k &= \boldsymbol{W}_k^H \boldsymbol{Y}_k, \\ \boldsymbol{W}_k &= (\boldsymbol{\Pi}_k \boldsymbol{\Pi}_k^H + \frac{\sigma_n^2}{\sigma_s^2} \boldsymbol{I}_{N_c})^{-1} \boldsymbol{\Pi}_k, \\ \boldsymbol{\Pi}_k &= \boldsymbol{\Pi}(\boldsymbol{\mathcal{I}}_k, \boldsymbol{\mathcal{I}}_k), \\ \boldsymbol{Y}_k &= \boldsymbol{Y}(\boldsymbol{\mathcal{I}}_k), \end{aligned} \tag{6}$$

where $\{\boldsymbol{W}_k = \{\boldsymbol{w}_{k,n'} | n' = 1, ..., N_c\} | k = 1, ..., K\}$ are K banks of filters where $\boldsymbol{w}_{k,n'}$ is the filter for the k-th user's n'-th subcarrier. $\boldsymbol{z}_k$ is the detected soft symbol vector of the k-th user. The mapping between the overall subcarrier index n and $\{k, n'\}$ is given by

$$n = \boldsymbol{\mathcal{I}}_k(n').$$

The entries of $\mathbf{\Pi}_k \in \mathcal{C}^{N_c \times N_c}$ and $\boldsymbol{Y}_k \in \mathcal{C}^{N_c \times 1}$ are selected from $\mathbf{\Pi}$ and $\boldsymbol{Y}$, respectively, according to the index vector $\boldsymbol{\mathcal{I}}_k$, which records the indices of subcarriers assigned to the k-th user. Fig. 1 illustrates the entry selection of $\mathbf{\Pi}_k$ for both the SCAS and the GCAS. Note that Fig. 1 (a) is shared by the SCG method regardless of the CAS, which will be detailed in the next subsection. In this case, for example, if the j-th, m-th and n-th subcarriers (recorded in $\boldsymbol{\mathcal{I}}_k$) are assigned to the k-th user, the entries marked with the cross shadow in the figure are selected. The difference between the SCAS and the GCAS is that $\mathbf{\Pi}_k$ for the SCAS is the sub-matrix on the diagonal of $\mathbf{\Pi}$ while the entries of $\mathbf{\Pi}_k$ for the GCAS are randomly distributed in $\mathbf{\Pi}$.

B. Subcarrier-Grouped Method

In the SCG method, we organize adjacent subcarriers into groups. Suppose that the number of subcarriers in a group is N_{sc} and the number of groups then is $G = N/N_{sc}$. Thus, the g-th group contains the indices of subcarriers from $(g-1)N_{sc}+1$ to gN_{sc} whose index vector is denoted as $\boldsymbol{\mathcal{I}}_g, g = 1, ..., G$, and there is no difference between the detectors for the SCAS and the GCAS scenarios. Without loss of generality, the detection of the g-th group is mathematically given by

$$\begin{aligned} \boldsymbol{z}_g &= \boldsymbol{W}_g^H \boldsymbol{Y}_g, \\ \boldsymbol{W}_g &= (\mathbf{\Pi}_g \mathbf{\Pi}_g^H + \frac{\sigma_n^2}{\sigma_s^2} \boldsymbol{I}_{N_{sc}})^{-1} \mathbf{\Pi}_g, \\ \mathbf{\Pi}_g &= \mathbf{\Pi}(\boldsymbol{\mathcal{I}}_g, \boldsymbol{\mathcal{I}}_g), \\ \boldsymbol{Y}_g &= \boldsymbol{Y}(\boldsymbol{\mathcal{I}}_g), \end{aligned} \tag{7}$$

where $\boldsymbol{z}_g$ denotes the detected soft symbol vector with the order of N_{sc} for the g-th group, where $g = 1, ..., G$ the entries of $\mathbf{\Pi}_g \in \mathcal{C}^{N_{sc} \times N_{sc}}$ and $\boldsymbol{Y}_g \in \mathcal{C}^{N_{sc} \times 1}$ are selected from $\mathbf{\Pi}$ and $\boldsymbol{Y}$, respectively, according to the index vector $\boldsymbol{\mathcal{I}}_g$, which records the indices of adjacent subcarriers grouped into the g-th group. $\{\boldsymbol{W}_g = \{\boldsymbol{w}_{g,n'} | n' = 1, ..., N_{sc}\} | g = 1, ..., G\}$ are G banks of filters where $\boldsymbol{w}_{g,n'}$ is the filter for the n'-th subcarrier in the g-th group. The mapping between the overall subcarrier index n and $\{g, n'\}$ is given by

$$n = \boldsymbol{\mathcal{I}}_g(n').$$

The entry selection of $\mathbf{\Pi}_g$ is illustrated in Fig. 1 (a) where the entries marked with the cross shadow are selected. Note that $\{\mathbf{\Pi}_g | g = 1, ..., G\}$ are G sub-matrices of $\mathbf{\Pi}$ and locate on its diagonal.

The explicit differences between the UG-MMSE and SCG-MMSE detectors, which are reflected in equations (6) and (7), are the subscripts k/g and the index vector $\mathcal{I}_k/\mathcal{I}_g$. But the inherent difference between these two algorithms, which we are claiming, is the way to organize a group. Different grouping method would bring different features into the algorithm.

IV. Proposed Multi-stage Interference Cancellation Scheme

Besides the advantage of low-complexity which thanks to the small size matrix inversion, another advantage of the G-MMSE algorithm is that we can reuse the filters $\{\boldsymbol{W}_k|k=1,...,K\}$ for the UG method or $\{\boldsymbol{W}_g|g=1,...,G\}$ for the SCG method in the subsequent IC stages. As a result, the system performance can be greatly improved, without causing significant complexity increase. In this section, we will discuss the proposed UG-MMSE-MIC and SCG-MMSE-MIC schemes with the novel IC strategy, respectively.

A. UG-MMSE-MIC scheme

The diagram of the proposed multi-stage interference cancellation scheme is depicted in Fig. 2, which can be shared by both the UG-MMSE-MIC and the SCG-MMSE-MIC schemes. In the UG method case, the proposed UG-MMSE-MIC scheme concatenates the UG-MMSE detector, shown as $\boldsymbol{W}_1,...,\boldsymbol{W}_K$, with multiple IC units, whose pseudo code is given in Table I (a). Each IC unit reuses K banks of filters $\{\boldsymbol{W}_k|k=1,...,K\}$ in the UG-MMSE detector. Let $\hat{\boldsymbol{s}}_k^{(m)}$ denotes the restored symbol vector obtained by

$$\hat{\boldsymbol{s}}_k^{(m)} = \mathrm{Restore}(\boldsymbol{z}_k^{(m)}), \tag{8}$$

where $\mathrm{Restore}(\boldsymbol{z}_k^{(m)})$ denotes the operator of restoring the symbol from the detected symbol $\boldsymbol{z}_k^{(m)}$, which contains demodulation and remodulation operations. The restored symbol vector $\hat{\boldsymbol{s}}_k^{(m)}$ for the k-th user at the output of the m-th IC unit , will be sent to the $(m+1)$-th IC unit, where $m=1,...,M$ and M is the total number of IC units. $\hat{\boldsymbol{s}}_k^{(0)}$ is the restored symbol vector for the k-th user from the UG-MMSE detector, which is sent to the first IC unit. In Table I (a), we formalize the pseudo code of the m-th IC unit, where without loss of generality, we take example of the k-th user. Firstly, $\boldsymbol{s}^m$ with the order of N is initialized to zero vector. Then, $K-1$ users' restored symbol vectors $(\hat{\boldsymbol{s}}_1^{(m-1)},...,\hat{\boldsymbol{s}}_{k-1}^{(m-1)},\hat{\boldsymbol{s}}_{k+1}^{(m-1)},...,\hat{\boldsymbol{s}}_K^{(m-1)})$, which are detected from the $(m-1)$th IC unit, are mapped into $\boldsymbol{s}^m$ except the k-th user. Subsequently, by

subtracting the reconstructed signal of all other users from the received frequency-domain signal vector, the signal $\boldsymbol{Y}^{(m)}$, which theoretically contains only the k-th user is obtained. Reusing the UG-MMSE detector $\boldsymbol{W}_k$ on $\boldsymbol{Y}_k^{(m)}$, which is formed by selecting entries from $\boldsymbol{Y}^{(m)}$ according to $\boldsymbol{\mathcal{I}}_k$, we can get the detected symbol vector for the k-th user. It is worth noting that the 7-th line of the pseudo-code not only sends the restored symbol vector to the output of current IC stage, which will be used in the next IC unit, but also updates the restored symbol vector of current IC unit, which will improve the subsequent detection of other users. This makes an important difference between our proposed MIC scheme with the conventional PIC scheme. Although conventional PIC scheme has less latency, our proposed UG-MMSE-MIC scheme can provide much better performance. Note that the HLCC scheme, which applies the conventional multi-stage PIC structure, will be compared with the proposed scheme in the simulations.

B. SCG-MMSE-MIC scheme

For the SCG method case, as depicted in Fig. 2, the proposed SCG-MMSE-MIC scheme concatenates the SCG-MMSE detector, shown as $\boldsymbol{W}_1, ..., \boldsymbol{W}_G$, with multiple IC units, whose pseudo code is given in Table I (b). Let $\hat{\boldsymbol{s}}_g^{(m)}$ denote the restored symbol vector for the g-th group at the output of the m-th IC unit, which will be sent to the $(m+1)$-th IC unit, where $m = 1, ..., M$ and M is the total number of IC units. $\hat{\boldsymbol{s}}_g^{(0)}$ is the restored symbol vector for the g-th group from the SCG-MMSE detector, which is sent to the first IC unit. In Table I (b), we formalize the pseudo code of the m-th IC unit, where without loss of generality, we take the g-th group as example. Similar with the UG-MMSE-MIC scheme, the 7-th line of the pseudo-code not only sends the restored symbol vector to the output of current IC stage, which will be used in the next IC unit, but also updates the detected symbol vector of current IC unit, which will improve the subsequent detection of other groups.

V. THEORETICAL ANALYSIS

In this section, both complexity analysis in terms of the number of multiplications and additions and bit error probability (BEP) analysis according to the signal-to-interference-plus-noise ratio (SINR) are carried out. The complexity of both the UG-MMSE-MIC and SCG-MMSE-MIC schemes are analysed, respectively, due to their different nature of processing. For the performance analysis, only the SCG-MMSE and SCG-MMSE-MIC algorithms are considered

because the procedures for BEP analysis of the UG method is exactly the same with the SCG method.

A. *Complexity Analysis*

The computational complexity of our proposed UG-MMSE-MIC and SCG-MMSE-MIC schemes in terms of the number of multiplications and additions ~~are~~ is compared with other existing schemes, namely the CLJL [16], the HLCC [10], the FMMSE and the BMMSE schemes [18], and given in Table II. In these schemes, the CLJL is the simplest scheme with the complexity of $\mathcal{O}(KN_c^2)$, however it provides the worst detection performance as will be shown in the simulations. The HLCC and the proposed UG-MMSE-MIC have comparable computational complexity, which is $\mathcal{O}(MKN^2)$. The proposed SCG-MMSE-MIC scheme has complexity of $\mathcal{O}(MGN^2)$, which is related to the number of groups. The FMMSE scheme has the highest complexity of $\mathcal{O}(N^3)$ and the BMMSE scheme, whose complexity of $\mathcal{O}(N\tau^2)$ is determined by the parameter τ, is a complexity efficient algorithm to approximate the FMMSE scheme. Note that the complexity of the CLJL, the HLCC and the proposed UG-MMSE-MIC algorithms are related to the parameters K and N_c. This means that once the number of users and the number of subcarriers allocated to a single user are fixed at the transmitter side, the complexity of the receiver using these three algorithms is fixed, as shown in Table II. ~~While the complexity of the proposed SCG-MMSE-MIC scheme, which is independent to K and N_c, is determined by flexible parameter N_{sc} and corresponding G, which can be selected to achieve the best trade-off.~~ Unlike the above algorithms, the complexity of the proposed SCG-MMSE-MIC scheme is flexible since it is determined by N_{sc} and corresponding G rather than K and N_c. Thus, in this case, we may have the freedom to achieve the best trade-off between performance and the complexity by selecting N_{sc}. We compare the proposed schemes with the existing schemes in two different ways. Firstly, the required operations of multiplications and additions for the proposed UG-MMSE-MIC scheme and other existing schemes are illustrated using the bar chart in Fig. 3 (a) with a system setting of N=128, K=8, N_c=16. According to [10], [18], the number of IC stages M is equal to 2 and τ is set to 30 to provide reasonable performance. Note that although the complexity of the proposed scheme is slightly higher than the HLCC scheme, as will be shown in the simulations, it outperforms other existing schemes including the FMMSE scheme. Secondly, the required operations of multiplication and addition against N_{sc} for the proposed SCG-MMSE-

MIC scheme and other existing schemes are illustrated in Fig. 3 (b) with a system setting of N=128. The number of IC stages M and τ are also equal to 2 and 30, respectively. It is worth emphasizing that in the figure N_{sc} for all algorithms except the SCG-MMSE-MIC represents N_c and only the value of N_{sc} for the SCG-MMSE-MIC scheme can be chosen at the receiver end. For example, N_{sc}=4 in the figure means that N_c=4 and K=32 for all other algorithms while the SCG-MMSE-MIC scheme can configure the parameters to achieve the best trade-off between the performance and the complexity regardless of K and N_c. As illustrated in Fig. 3 (b), for example, for a system with 32 users (K=32, N_c=4), the complexity of the HLCC algorithms has N_{sc}=4 with 9.86E+5 multiplications and 1.05E+6 additions, while the SCG-MMSE-MIC scheme can employ N_{sc} = 16 so that it only requires 3.05E+5 multiplications and 2.95E+5 additions.

B. Performance Analysis

This subsection presents theoretical performance analysis of the G-MMSE detector and G-MMSE-MIC scheme. The analysis is motivated by the performance studies of PIC in [24] where the error probability is analysed in terms of the SINR. In order to present the complex analysis procedure clearly, we divide the analytical task into three steps: the first step is the BEP analysis of the G-MMSE detector, the second is the BEP analysis of the G-MMSE-MIC schemes with perfect IC, and the third is the BEP analysis of the G-MMSE-MIC schemes with IC errors. Since the main difference between the UG-MMSE and SCG-MMSE schemes is the use of the subscript k/g and the index vector $\boldsymbol{\mathcal{I}}_k/\boldsymbol{\mathcal{I}}_g$, which would not affect the performance analysis, we only present here the analysis of the SCG-MMSE detector and SCG-MMSE-MIC scheme.

1) SCG-MMSE Detector: Let us denote the average BEP of the G-MMSE detector as $\bar{\mathrm{P}}^G$, which is given by

$$\bar{\mathrm{P}}^G = \frac{1}{N}\sum_{n=1}^{N}\left[\int_{\mathcal{H}_n}\int_{\boldsymbol{\epsilon}} \mathrm{Pe}_n^G(\boldsymbol{\Pi})p(\mathcal{H}_n)p(\boldsymbol{\epsilon})d\mathcal{H}_n d\boldsymbol{\epsilon}\right],$$

$$\bar{\mathrm{P}}^G = \frac{1}{N}\sum_{n=1}^{N}\left[\int_{\mathcal{H}_n}\int_{\boldsymbol{\epsilon}} \mathrm{Pe}_n^G(\boldsymbol{\Pi}|\mathcal{H}_n,\boldsymbol{\epsilon})p(\mathcal{H}_n)p(\boldsymbol{\epsilon})d\mathcal{H}_n d\boldsymbol{\epsilon}\right], \tag{9}$$

where $\mathrm{Pe}_n^G(\boldsymbol{\Pi}|\mathcal{H}_n,\boldsymbol{\epsilon})$ denotes the BEP of the G-MMSE detector on the n-th subcarrier conditioned on the CFR $\boldsymbol{H}$ and the CFOs $\boldsymbol{\epsilon}$, since $\boldsymbol{\Pi}$ is determined by $\boldsymbol{H}$ and $\boldsymbol{\epsilon}$ according to (3), $p(\mathcal{H}_n)$ and $p(\boldsymbol{\epsilon})$ are the probability density functions (PDFs) of the fading amplitude on the n-th

subcarrier and the CFOs, respectively. Because it is impossible to derive a close form to evaluate the error probability, ~~our method is to average the EP over the channel and CFOs as many as possible in a Monte-Carlo fashion.~~ we employ a semi-theoretical method to divert the problem from calculating BEP conditioned on the PDFs of channel and CFOs theoretically. We generate L sets of channel coefficients and CFOs randomly as we did for Monte-Carlo simulation. The semi-theoretical BEP is then calculated directly rather than counting the BER. The final BEP is averaged over L sets of channels and CFOs. If $L \to \infty$, the semi-theoretical analysis will be approximated to theoretical one. Note that for given $\boldsymbol{H}$ and the CFOs $\boldsymbol{\epsilon}$, $\boldsymbol{\Pi}$ is fixed. Thus, since the CFOs are uniformly distributed, the average BEP $\bar{\mathrm{P}}^G$ can be approximated to

$$\bar{\mathrm{P}}^G \approx \frac{1}{N}\sum_{n=1}^{N}\left[\int_{\mathcal{H}_n} \mathrm{Pe}_n^G(\boldsymbol{\Pi}) p(\mathcal{H}_n) d\mathcal{H}_n\right], \approx \frac{1}{N}\sum_{n=1}^{N}\left[\lim_{L\to\infty}\sum_{i=1}^{L}\mathrm{Pe}_n^G\left(\boldsymbol{\Pi}(i)\right) p\left(\mathcal{H}_n(i)\right)\right],$$

$$\bar{\mathrm{P}}^G \approx \frac{1}{N}\sum_{n=1}^{N}\left[\lim_{L\to\infty}\frac{1}{L}\sum_{i=1}^{L}\mathrm{Pe}_n^G\left(\boldsymbol{\Pi}(i)|\mathcal{H}_n(i),\boldsymbol{\epsilon}(i)\right)\right], \tag{10}$$

where $\boldsymbol{\Pi}(i)$ is for the i-th block transmission.

As is well known that in a multicarrier system, a frequency-selective fading channel is viewed as several independent frequency-flat fading subchannels on individual subcarriers. We assume that the fading amplitude of each frequency-flat fading subchannel satisfies Rayleigh distribution.

In this case, the frequency-domain received signal vector $\boldsymbol{Y}(i)$ for the i-th block in (3) can be further re-written as

$$\begin{aligned}\boldsymbol{Y}(i) = &\overbrace{\boldsymbol{\Pi}^{(\mathcal{I}_g(n'))}(i)s^{(\mathcal{I}_g(n'))}(i)}^{\boldsymbol{\mathcal{S}}_{g,n'}(i)} \\ &+ \overbrace{\sum_{\substack{\tilde{n}=1 \\ \tilde{n}\neq\mathcal{I}_g(n')}}^{N}\boldsymbol{\Pi}^{(\tilde{n})}(i)s^{(\tilde{n})}(i) + \boldsymbol{v}(i)}^{\boldsymbol{\mathcal{V}}_{g,n'}^G(i)},\end{aligned} \tag{11}$$

where $\boldsymbol{\Pi}^{(n)}(i)$ denotes the n-th column of the matrix $\boldsymbol{\Pi}(i)$ and $s^{(n)}(i)$ denotes the n-th element in the vector $\boldsymbol{s}(i)$, the frequency-domain received signal of the n'-th subcarrier in the g-th group is denoted as $\boldsymbol{\mathcal{S}}_{g,n'}(i)$ and the corresponding interference caused by other subcarriers plus noise is denoted as $\boldsymbol{\mathcal{V}}_{g,n'}^G(i)$. Let us assume that the interference-plus-noise $\boldsymbol{\mathcal{V}}_{g,n'}^G(i)$ is Gaussian distributed. The assumption is reasonable because of central limit theorem. Under our system

$$\bar{\mathrm{P}}^{\mathrm{G}} = \frac{1}{N}\sum_{n=1}^{N}\left[\lim_{L\to\infty}\frac{1}{L}\sum_{i=1}^{L}\mathbf{Q}\left(\sqrt{2\frac{\mathbb{E}\left[|\boldsymbol{w}_n^H(i)\boldsymbol{\mathcal{S}}_n(i,\boldsymbol{\mathcal{I}}_g)|^2\right]}{\mathbb{E}\left[|\boldsymbol{w}_n^H(i)\boldsymbol{\mathcal{V}}_n^G(i,\boldsymbol{\mathcal{I}}_g)|^2\right]}}\right)\underline{p\left(\mathcal{H}_n(i)\right)}\right] \tag{15}$$

model, the output of the SCG-MMSE detector for the n'-th subcarrier in the g-th group is written as

$$\begin{aligned} z_{g,n'}(i) &= \boldsymbol{w}_{g,n'}^H(i)\boldsymbol{Y}_g(i) \\ &= \boldsymbol{w}_{g,n'}^H(i)\boldsymbol{\mathcal{S}}_{g,n'}(i,\boldsymbol{\mathcal{I}}_g) + \boldsymbol{w}_{g,n'}^H(i)\boldsymbol{\mathcal{V}}_{g,n'}^G(i,\boldsymbol{\mathcal{I}}_g). \end{aligned} \tag{12}$$

According to the mapping between n and $\{g,n'\}$, the SINR for the n-th subcarrier can be given by

$$\gamma_{n|\boldsymbol{\Pi}(i)}^G = \frac{\mathbb{E}\left[|\boldsymbol{w}_n^H(i)\boldsymbol{\mathcal{S}}_n(i,\boldsymbol{\mathcal{I}}_g)|^2\right]}{\mathbb{E}\left[|\boldsymbol{w}_n^H(i)\boldsymbol{\mathcal{V}}_n^G(i,\boldsymbol{\mathcal{I}}_g)|^2\right]}, \tag{13}$$

where $\mathbb{E}[\cdot]$ donotes the expectation operator. According to [24], [25], the BEP $\mathrm{Pe}_n^G(\boldsymbol{\Pi}(i)|\mathcal{H}_n(i),\boldsymbol{\epsilon}(i))$ can be easily obtained by

$$\mathrm{Pe}_n^G(\boldsymbol{\Pi}(i)|\mathcal{H}_n(i),\boldsymbol{\epsilon}(i)) = \mathbf{Q}(\sqrt{2\gamma_{n|\boldsymbol{\Pi}(i)}^G}), \tag{14}$$

where $\gamma_{n|\boldsymbol{\Pi}(i)}^G$ denotes the SINR of the symbol carried on the n-th subcarrier with given $\boldsymbol{\Pi}(i)$ and

$$\mathbf{Q}(x) \triangleq \frac{1}{\sqrt{2\pi}}\int_x^\infty e^{-t^2/2}dt.$$

By substituting (13) into (14) and then (10), we can obtain the average BEP $\bar{\mathrm{P}}^G$ for the SCG-MMSE detector as (15).

2) SCG-MMSE-MIC Scheme With Perfect IC: In the perfect IC case, the interference from other groups are perfectly cancelled, thus, the frequency-domain post perfect IC (PPIC) signal vector $\boldsymbol{Y}^{\mathrm{PPIC}}$ can be written as

$$\begin{aligned} \boldsymbol{Y}^{\mathrm{PPIC}}(i) = &\overbrace{\boldsymbol{\Pi}^{(\boldsymbol{\mathcal{I}}_g(n'))}(i)s^{(\boldsymbol{\mathcal{I}}_g(n'))}(i)}^{\boldsymbol{\mathcal{S}}_{g,n'}(i)} \\ &+ \overbrace{\sum_{\substack{\tilde{n}=1\\ \tilde{n}\neq n'}}^{N_{sc}}\boldsymbol{\Pi}^{(\boldsymbol{\mathcal{I}}_g(\tilde{n}))}(i)s^{(\boldsymbol{\mathcal{I}}_g(\tilde{n}))}(i) + \boldsymbol{v}(i)}^{\boldsymbol{\mathcal{V}}_{g,n'}^{\mathrm{PPIC}}(i)}. \end{aligned} \tag{16}$$

$$\bar{\mathrm{P}}^{\mathrm{PPIC}} = \frac{1}{N}\sum_{n=1}^{N}\left[\lim_{L\to\infty}\frac{1}{L}\sum_{i=1}^{L}\mathbf{Q}\left(\sqrt{2\frac{\mathbb{E}\left[|\boldsymbol{w}_n^H(i)\boldsymbol{\mathcal{S}}_n(i,\boldsymbol{\mathcal{I}}_g)|^2\right]}{\mathbb{E}\left[|\boldsymbol{w}_n^H(i)\boldsymbol{\mathcal{V}}_n^{\mathrm{PPIC}}(i,\boldsymbol{\mathcal{I}}_g)|^2\right]}}\right)\underline{p\left(\mathcal{H}_n(i)\right)}\right] \tag{18}$$

The SINR of the n-th subcarrier for the SCG-MMSE-MIC scheme with perfect IC can be given by

$$\gamma_{n|\boldsymbol{\Pi}(i)}^{\mathrm{PPIC}} = \frac{\mathbb{E}\left[|\boldsymbol{w}_n^H(i)\boldsymbol{\mathcal{S}}_n(i,\boldsymbol{\mathcal{I}}_g)|^2\right]}{\mathbb{E}\left[|\boldsymbol{w}_n^H(i)\boldsymbol{\mathcal{V}}_n^{\mathrm{PPIC}}(i,\boldsymbol{\mathcal{I}}_g)|^2\right]}. \tag{17}$$

By substituting (17) into (14) and then (10), we can further obtain the average BEP of the SCG-MMSE-MIC scheme with perfect IC, as given by (18).

3) SCG-MMSE-MIC Scheme With IC Errors: The interference will be even enhanced when IC errors (ICE) occur in the $N - N_{sc}$ cancelled symbols. Let us define error event sets $\{\boldsymbol{E}_j | j = 0, 1, ..., N - N_{sc}\}$ for the case when j errors out of $N - N_{sc}$ symbols occurred in the current IC stage. The number of error events in the error event set $\boldsymbol{E}_j$ is $N_e = C(N - N_{sc}, j)$, that is $\boldsymbol{E}_j = \{e_j^c | c = 1, ..., N_e\}$, where $C(n, r)$ denotes the combination operator as $\binom{n}{r}$ and e_j^c denotes the c-th error event in the error event set $\boldsymbol{E}_j$. We can write the BEP of the SCG-MMSE-MIC scheme with ICE $\mathrm{Pe}_{n,m}^{\mathrm{ICE}}(\boldsymbol{\Pi}(i)|\mathcal{H}_n(i), \boldsymbol{\epsilon}(i))$ on the n-th subcarrier in the m-th IC unit for the i-th block. For simplicity, we drop $\mathcal{H}_n(i), \boldsymbol{\epsilon}(i)$ and write $\mathrm{Pe}_{n,m}^{\mathrm{ICE}}(\boldsymbol{\Pi}(i))$ as

$$\mathrm{Pe}_{n,m}^{\mathrm{ICE}}(\boldsymbol{\Pi}(i)) = \sum_{j=0}^{N-N_{sc}}\sum_{c=1}^{N_e}\mathrm{Pe}_n^{\mathrm{ICE}}\left\{\boldsymbol{\Pi}(i)|e_j^c\right\}\mathrm{P}_{m-1}\{e_j^c\}, \tag{19}$$

where $\mathrm{P}_{m-1}\{e_j^c\}$ is the probability for the error event e_j^c, which can be calculated based on the BEP from the $(m-1)$-th IC stage $\mathrm{Pe}_{n,m-1}^{\mathrm{ICE}}(\boldsymbol{\Pi}(i))$. Note that for the first IC stage ($m = 1$), $\mathrm{Pe}_{n,m-1}^{\mathrm{ICE}}(\boldsymbol{\Pi}(i))$ is $\mathrm{Pe}_n^{G}(\boldsymbol{\Pi}(i))$. $\mathrm{Pe}_n^{\mathrm{ICE}}\left\{\boldsymbol{\Pi}(i)|e_j^c\right\}$ is the BEP conditioned on the error event e_j^c, which can be written as

$$\mathrm{Pe}_n^{\mathrm{ICE}}\left\{\boldsymbol{\Pi}(i)|e_j^c\right\} = \mathbf{Q}(\sqrt{2\gamma_{n|\boldsymbol{\Pi}(i),e_j^c}^{\mathrm{ICE}}}), \tag{20}$$

where $\gamma_{n|\boldsymbol{\Pi}(i),e_j^c}^{\mathrm{ICE}}$ is the SINR conditioned on the error event e_j^c. To calculate $\gamma_{n|\boldsymbol{\Pi}(i),e_j^c}^{\mathrm{ICE}}$, we can write the frequency-domain signal vector conditioned on the error event e_j^c as $\boldsymbol{Y}_{e_j^c}^{\mathrm{ICE}}(i)$ in (21), where the second item of $\boldsymbol{\mathcal{V}}_{g,n'|e_j^c}^{\mathrm{ICE}}(i)$ denotes the extra interference caused by the error event e_j^c. Thus, $\gamma_{n|\boldsymbol{\Pi}(i),e_j^c}^{\mathrm{ICE}}$ is given by

$$\gamma_{n|\boldsymbol{\Pi}(i),e_j^c}^{\mathrm{ICE}} = \frac{\mathbb{E}\left[|\boldsymbol{w}_n^H(i)\boldsymbol{\mathcal{S}}_n(i,\boldsymbol{\mathcal{I}}_g)|^2\right]}{\mathbb{E}\left[|\boldsymbol{w}_n^H(i)\boldsymbol{\mathcal{V}}_{n|e_j^c}^{\mathrm{ICE}}(i,\boldsymbol{\mathcal{I}}_g)|^2\right]}. \tag{22}$$

$$\boldsymbol{Y}^{\text{ICE}}_{e^c_j}(i) = \overbrace{\boldsymbol{\Pi}^{(\boldsymbol{\mathcal{I}}_g(n'))}(i)s^{(\boldsymbol{\mathcal{I}}_g(n'))}(i)}^{\boldsymbol{\mathcal{S}}_{g,n'}(i)} + \overbrace{\sum_{\substack{\tilde{n}=1 \\ \tilde{n}\neq n'}}^{N_{sc}} \boldsymbol{\Pi}^{(\boldsymbol{\mathcal{I}}_g(\tilde{n}))}(i)s^{(\boldsymbol{\mathcal{I}}_g(\tilde{n}))}(i) + \sum_j 2\boldsymbol{\Pi}^{(n_j)}(i)s^{(n_j)}(i) + \boldsymbol{v}(i)}^{\boldsymbol{\mathcal{V}}^{\text{ICE}}_{g,n'|e^c_j}(i)}. \tag{21}$$

Similar with (9), we can write the average BEP of the proposed SCG-MMSE-MIC scheme for the m-th IC unit $\bar{\text{P}}^{\text{ICE}}_m$ as

$$\bar{\text{P}}^{\text{ICE}}_m = \frac{1}{N}\sum_{n=1}^{N}\left[\lim_{L\to\infty}\frac{1}{L}\sum_{i=1}^{L}\text{Pe}^{\text{ICE}}_{n,m}(\boldsymbol{\Pi}(i))\underline{p\left(\mathcal{H}_n(i)\right)}\right]. \tag{23}$$

To explain our performance analysis clearly, we take an example of a small system. Let us consider a system with N=8 subcarriers, N_{sc}=4 subcarriers in each group and G=2 groups. Suppose we are calculating the BEP for the third subcarrier (n=3), which is supposed to locate in the first group. Thus, the IC errors will only occur in the second group and the possible number of errors j is from 0 to $N - N_{sc}$, in this case, is 4. When there are j erroneous subcarriers out of 4 subcarriers, N_e will be $\binom{4}{j}$ possible combinations of erroneous subcarriers, say j=2, then N_e=6. The error event set $\boldsymbol{E}_2$ contains 6 error events $\{e^c_2|c = 1, ..., 6\}$ where $\{e^1_2 = \{5,6\}, e^2_2 = \{5,7\}, e^3_2 = \{5,8\}, e^4_2 = \{6,7\}, e^5_2 = \{6,8\}, e^6_2 = \{7,8\}\}$. To calculate $\text{Pe}^{\text{ICE}}_{3,1}(\boldsymbol{\Pi}(i))$ for the first IC stage (m=1), we have to take all error event sets into account and consider the BEPs of all the error events based on $\text{Pe}^G_n(\boldsymbol{\Pi}(i))$ as *a priori* probabilities. Based on *a priori* probability considering $1 - \text{Pe}^G_n(\boldsymbol{\Pi}(i))$ for correct subcarriers and $\text{Pe}^G_n(\boldsymbol{\Pi}(i))$ for erroneous subcarriers, we obtain the probability of the error event $\text{P}_0\{e^c_j\}$, for example, $\text{P}_0\{e^1_2\}$ is obtained by

$$\text{Pe}^G_5(\boldsymbol{\Pi}(i))\text{Pe}^G_6(\boldsymbol{\Pi}(i))(1 - \text{Pe}^G_7(\boldsymbol{\Pi}(i)))(1 - \text{Pe}^G_8(\boldsymbol{\Pi}(i))).$$

Using (20), (21) and (22), we can obtain $\text{Pe}^{\text{ICE}}_3\left\{\boldsymbol{\Pi}(i)|e^c_j\right\}$ conditioned on the error event e^c_j. By calculating error probabilities conditioned on all error events $\text{Pe}^{\text{ICE}}_3\left\{\boldsymbol{\Pi}(i)|e^c_j\right\}$ and their *a priori* probabilities $\text{P}_{m-1}\{e^c_j\}$ where $j = 1, ..., N - N_{sc}$, $c = 1, ..., N_e$, and substituting them into (19), we can obtain $\text{Pe}^{\text{ICE}}_{3,1}(\boldsymbol{\Pi}(i))$. The average BEP for the first IC stage is obtained by averaging $\text{Pe}^{\text{ICE}}_{n,1}(\boldsymbol{\Pi}(i))$ over all N subcarriers and all the blocks according to (23).

VI. Simulation Results

In this section, numerical results of the proposed schemes including both the UG-MMSE-MIC and SCG-MMSE-MIC schemes are reported. Consider an OFDMA uplink system with N=128 subcarriers and both uncoded binary phase-shift keying (BPSK) and quadrature phase-shift keying (QPSK) modulations, which is operating in the 5 GHz frequency band and the subcarrier spacing equal to 10.94 kHz. Considering that $N_0 \neq 0$ zero carrier guards placed at both edges of signal spectrum in the practical system improve the performance, we investigate the system with $N_0 = 0$ as the worst case. That means each frame contains 128 symbols. The channel coefficients and CFOs change frame by frame. Both the SCAS and the GCAS are employed as the subcarrier allocation scheme for the UG-MMSE-MIC scheme and only the GCAS is considered for the SCG-MMSE-MIC scheme because with the SCAS, the SCG-MMSE-MIC scheme is similar with the UG-MMSE-MIC scheme. We define two scenarios for the investigation: scenario one employs $K = 8$ and $N_c = 16$, and scenario two employs $K = 32$ and $N_c = 4$. The channel between each user and the BS is assumed invariant within one block, but may change independently from one block to the next. The length of the channel N_h is 8 and the average power of each tap follows exponential power delay profile given by

$$\mathbb{E}\left[|h_k^l|^2\right] = e^{-l/N_h}, \quad 0 \leq l \leq N_h - 1, \tag{24}$$

where $\mathbb{E}[\cdot]$ denotes the expectation operator. The length of CP is N_p=8. The normalized CFOs are randomly selected from $[-0.5, 0.5)$. We evaluate the performance of the proposed schemes in terms of the bit error rate (BER) against the signal-to-noise ratio (SNR). The SNR is defined as

$$\text{SNR} = 10 \log_{10} \frac{\sigma_s^2}{\sigma_n^2}. \tag{25}$$

All simulation results are averaged over 5000 independent frame iterations. In the rest of this section, we will firstly show the BER against SNR performance of the proposed schemes and other existing schemes in the system with perfect CFO estimation for both BPSK and QPSK modulations. Secondly, we will show the performance of the proposed schemes in the system with CFO estimation errors. At last, the analytical performance is given and validated by the simulation results.

A. With Perfect CFO Estimation

In this part, we assume that the CFO estimation is perfect. For the proposed UG-MMSE-MIC scheme, we firstly consider the uplink OFDMA systems employing the SCAS and the BPSK signal. Fig. 4 compares the BER performance of all the discussed schemes for the OFDMA uplink system with the scenario one. It is shown that the proposed UG-MMSE-MIC scheme has superior performance. The performance at the first IC unit of the proposed scheme has slightly better performance than other existing schemes, even including the FMMSE scheme. There is more than 1 dB SNR gain between the UG-MMSE-MIC scheme with two IC units and the FMMSE scheme at the BER level of 1E-3. The performance of the proposed scheme with two IC units is very close to that of the system without CFO when the SNR is lower than 25 dB.

Next, the BER performance of the UG-MMSE-MIC scheme, the SCG-MMSE-MIC scheme and all the discussed schemes is investigated for the OFDMA uplink system with the GCAS and the BPSK signal in the scenario one. In Fig. 5, the plots show that although the UG-MMSE detector has a similarly inferior performance as the CLJL scheme, with the concatenated IC units, the performance of the UG-MMSE-MIC scheme is greatly improved. At the BER level of 0.007, the performance at the output of the first IC unit (m=1) has nearly 5 dB SNR gain against the BMMSE scheme, nearly 3 dB gain against the HLCC scheme with two IC stages (m=2), and nearly 1 dB gain against the FMMSE scheme, respectively. Concatenating one more IC unit (m=2) produces more than 5 dB SNR gain at the BER level of 0.002, compared to the UG-MMSE-MIC scheme with one IC unit. On the other hand, the plot also shows that the SCG-MMSE detector has better performance than the CLJL scheme and the HLCC scheme with one IC stage and the performance is further improved when IC units are used. At the BER level of 0.005, the performance at the output of the first IC unit (m=1) has nearly 3 dB SNR gain against both the BMMSE scheme and the HLCC scheme with two IC stages (m=2). Concatenating one more IC unit (m=2) produces more than 5 dB SNR gain at the BER level of 0.001. The SCG-MMSE-MIC scheme with two IC units has comparable performance with the FMMSE when the SNR level is lower than 30 dB. The FMMSE scheme performs better than the UG-MMSE-MIC scheme with two IC units when the SNR level is higher than 28 dB. But depending on the requirement of the system performance, we can simply concatenate more IC units to improve the performance, without increasing the complexity significantly.

Furthermore, the plot also shows that the UG-MMSE-MIC scheme performs better when the SNR is lower than around 28 dB but the SCG-MMSE-MIC scheme is better at high SNR level. As we know that the detector is typically operated at low to moderate SNR region for the coded systems, so the UG-MMSE-MIC scheme is more suitable for the coded systems. Note that for the GMMSE detector without IC, the SCG method has better performance than the UG method. In the SCG method, the group is formed according to adjacent subcarriers, where the central subcarriers are protected from other groups, thus the interference from other groups is much lower than the UG method because in the UG method, each subcarrier in one group possibly is interfered by its neighboring subcarriers, which ~~are located~~ locate in other groups (allocated to different users). However, the situation is different when the IC units are employed. The interference from other groups is cancelled so that the interference coming from the same group becomes dominant. Since the inter-group interference of the UG method is much smaller than the SCG method, UG-MMSE-MIC becomes better. On the other hand, the performance of the UG-MMSE-MIC also depends on the performance of the previous stage of detection or IC. Thus, with the increase of the SNR, because the residual interference caused by detection errors of the UG method is larger than that of the SCG method, the UG-MMSE-MIC produces an error floor. That is the reason why there is a crossover between SCG-MMSE-MIC and UG-MMSE-MIC, and why the UG-MMSE-MIC performs better for low SNR and the SCG-MMSE-MIC is better at high SNR.

In Fig. 6, we examine the proposed scheme in the scenario two using two parameter settings, N_{sc}=4 and N_{sc}=16, denoted as S1 and S2, respectively. Clearly, the proposed scheme with N_{sc}=16 performs better than that with N_{sc}=4. The complexity of the scheme with N_{sc}=16 is also much lower than that of N_{sc}=4 according to the results in Fig. 3 (b). That is, the flexibility of the proposed scheme allows us to choose the optimal value for N_{sc} to achieve the best trade-off between the performance and complexity.

We also investigate the BER performance of the proposed schemes and all the discussed schemes for the OFDMA uplink system with the GCAS and the QPSK signal. The results shown in Fig. 7 indicate that the proposed algorithms perform also very well with higher order modulation. Compared with the results of the BPSK signal, the performance of the QPSK signal has a 3 dB right-shift, which is consistent to the theory.

B. With CFO Estimation Errors

In this part, we consider the case that CFO estimation errors exist. Suppose that CFO estimation has been accomplished by the methods in [14], [15]. The CFO estimation MSE is assumed to be [0.05, 0.003, 0.001, 0.0004, 0.00018, 0.0001, 0.00007, 0.00006, 0.00006] for the corresponding SNRs [0:5:40]. The results are shown in Fig. 8. The results indicate that with reasonable CFO estimation errors, the impact on the performance of all the algorithms is small.

C. Analytical Performance

To validate the performance analysis, the theoretical performance is evaluated for a simplified demonstration system with N=8 subcarriers, K=4 users, channel order N_h=4, N_{sc}=4 subcarriers in each group and G=2 groups, considering extremely high number of $C(n,r)$ operation when n is large. The theoretical results are shown in Fig. 9 in comparison with simulation results. The simulation results closely match the analytical results and effectively validate the theoretical analysis.

VII. Conclusions

In this paper, in order to achieve better trade-off between performance and complexity for the OFDMA uplink system, we proposed a grouped minimum mean squared error (G-MMSE) based multi-stage interference cancellation (MIC) scheme. The first stage of the proposed scheme is a G-MMSE detector, where the signal is detected group by group by a bank of partial MMSE filters. The grouping can be implemented according to either corresponding users or adjacent subcarriers, leading to the UG method and SCG method. By concatenating multiple novel IC units with the G-MMSE detector, the system performance is greatly improved. Since the filters in the G-MMSE detector can be reused in the subsequent IC units, the computational complexity is greatly reduced according to our complexity analysis. The BEP performance of the proposed scheme is theoretically analysed and validated by simulations. The numerical results show that the proposed G-MMSE-MIC schemes outperforms other existing schemes with considerable low complexity.

References

[1] I. Koffman and V. Roman, "Broadband wireless access solutions based on OFDM access in IEEE 802.16", IEEE Commun. Mag., vol. 40, no. 4, pp. 96 –103, Apr. 2002.

[2] Z. R. Cao, U. Tureli, and P. Liu, "Optimum subcarrier assignment for ofdma uplink", ACSSC, Nov. 2003, vol. 1, pp. 708 – 712 Vol.1.

[3] M. Morelli, "Timing and frequency synchronization for the uplink of an OFDMA system", IEEE Trans. Commun., vol. 52, no. 2, pp. 296-306, Feb. 2004.

[4] Z. R. Cao, U. Tureli, and Y.-D. Yao, "Deterministic multiuser carrier-frequency offset estimation for interleaved ofdma uplink", IEEE Trans. Commun., vol. 52, no. 9, pp. 1585-1594, Sept. 2004.

[5] Z. R. Cao, U. Tureli, Y.-D. Yao, and P. Honan, "Frequency synchronization for generalized OFDMA uplink", in Proc. IEEE Globecom Nov. 2004, vol. 2, pp. 1071-1075.

[6] K. Y. Kim, Y. N. Han, and S. L. Kim, "Joint subcarrier and power allocation in uplink ofdma systems", IEEE Commun. Lett., vol. 9, no. 6, pp. 526 – 528, jun 2005.

[7] M. Pun, M. Morelli, and C. Kuo, "Maximum-likelihood synchronization and channel estimation for OFDMA uplink transmissions," IEEE Trans. Commun., vol. 54, no. 4, pp. 726-736, April 2006.

[8] M. Morelli, C.-C.J. Kuo, and M.-O. Pun, "Synchronization techniques for orthogonal frequency division multiple access (OFDMA): A tutorial review", Proc. IEEE, vol. 95, no. 7, pp. 1394-1427, July 2007.

[9] D. Marabissi, R. Fantacci, and S. Papini, "Robust multiuser interference cancellation for OFDM systems with frequency offset", IEEE Trans. Wireless Commun., vol. 5, no. 11, pp. 3068-3076, Nov. 2006.

[10] D.-F. Huang and K. B. Letaief, "An interference-cancellation scheme for carrier frequency offsets correction in ofdma systems", IEEE Trans. Commun., vol. 53, no. 7, pp. 1155 – 1165, July 2005.

[11] S. Manohar, D. Sreedhar, V. Tikiya, and A. Chockalingam, "Cancellation of multiuser interference due to carrier frequency offsets in uplink ofdma", IEEE Trans. Wireless Commun., vol. 6, no. 7, pp. 2560-2571, July 2007.

[12] "IEEE Standard for Local and Metropolitan Area Networks, Part 16: Air Interface for Fixed Broadband Wireless Access Systems", IEEE Std. 802.16, Oct. 2004.

[13] H. Wang et al., "4G Wireless Video Communications", Wiley, 2009.

[14] Y. Zeng and A. Leyman, "Pilot-based simplified ML and fast algorithm for frequency offset estimation in OFDMA uplink", IEEE Trans. Veh. Technol., vol. 57, no. 3, pp. 1723C1732, May 2008.

[15] P.-F. Sun and L. Zhang, "Low complexity pilot aided frequency synchronization for OFDMA uplink transmission", IEEE Trans. Wireless Commun., vol. 8, no. 7, pp. 3758-3769, July 2009.

[16] J. Choi, C. Lee, H. W. Jung, and Y. H. Lee, "Carrier frequency offset compensation for uplink of OFDM-FDMA systems", IEEE Commun. Lett., vol. 4, no. 12, pp. 414-416, Dec. 2000.

[17] T. Yucek and H. Arslan, "Carrier frequency offset compensation with successive cancellation in uplink OFDMA systems", IEEE Trans. Wireless Commun., vol. 6, no. 10, pp. 3546-3551, Oct. 2007.

[18] Z. R. Cao, U. Tureli, and Y.-D. Yao, "Low-complexity orthogonal spectral signal construction for generalized OFDMA uplink with frequency synchronization errors", IEEE Trans. Veh. Tech. , vol. 56, no. 3, pp. 1143-1154, May 2007.

[19] S. Ahmed and L. Zhang, "Low complexity iterative detection for OFDMA uplink with frequency offsets", IEEE Trans. Wireless Commun., vol. 8, no. 3, pp. 1199-1205, March 2009.

[20] Van de Beek, J-J., Per Ola Borjesson, M-L. Boucheret, Daniel Landstrom, Julia Martinez Arenas, Per Odling, Christer Ostberg, Mattias Wahlqvist, and Sarah Kate Wilson, "A time and frequency synchronization scheme for multiuser OFDM IEEE Journal Sel. Areas Comm., 17.11 (1999): 1900-1914.

[21] A.-L. Johansson, L. K. Rasmussen, "Linear group-wise successive interference cancellation in CDMA", Proceed. Int. Sym. Spread Spec. Tech. App, 1998.

[22] L. Dai, S. Sfar and K. B. Letaief, "An Efficient Detector for Combined Space-time Coding and Layered Processing" IEEE Trans. Commun., v.53, no.9, pp. 1438 - 1442, Sept. 2005.

[23] G. H. Golub and C. F. van Loan, Matrix Computations, Wiley, 2002.

[24] D. R. Brown, M. Motani, V. Veeravalli, H. V. Poor, and C. R. Johnson, Jr., "On the performance of linear parallel interference cancellation", IEEE Trans. Inform. Theory, vol. 47, no. 5, pp. 1957-1970, July 2001.

[25] A. N. Barbosa, S. L. Miller, "Adaptive detection of DS/CDMA signals in fading channels", IEEE Trans. Commun. , v.46, no.1, pp.115-124, Jan 1998.

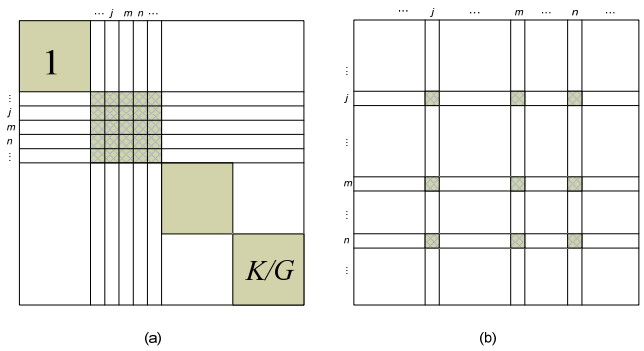

Fig. 1. (a) The illustration of entry selection, which can be shared by the UG method with the SCAS and the SCG method regardless of the CAS, and where K is the number of users for the UG method and G is the number of groups for the SCG method. (b) The illustration of entry selection for the k-th user's $\mathbf{\Pi}_k$ for the UG method with GCAS.

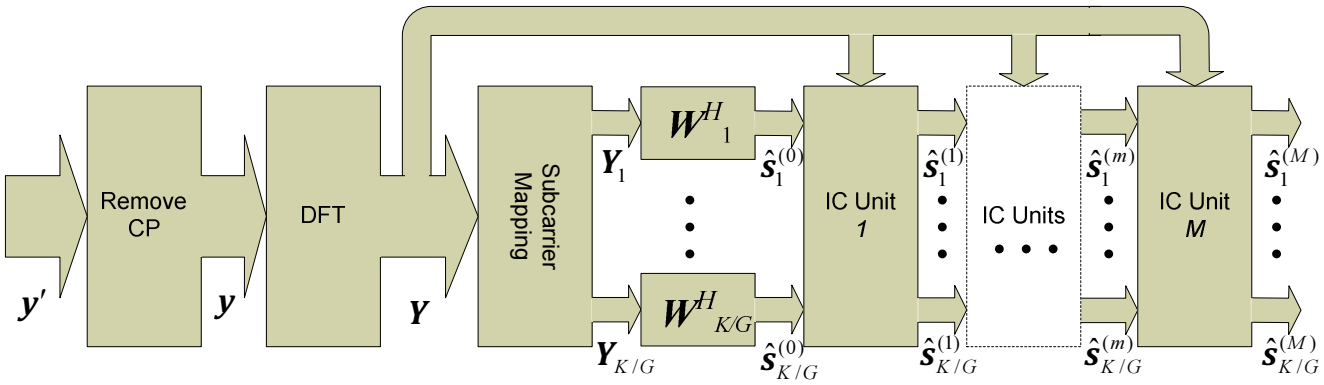

Fig. 2. The diagram of the proposed multi-stage interference cancellation scheme shared by both the UG-MMSE and SCG-MMSE algorithms, where K is the number of users for the UG method and G is the number of groups for the SCG method.

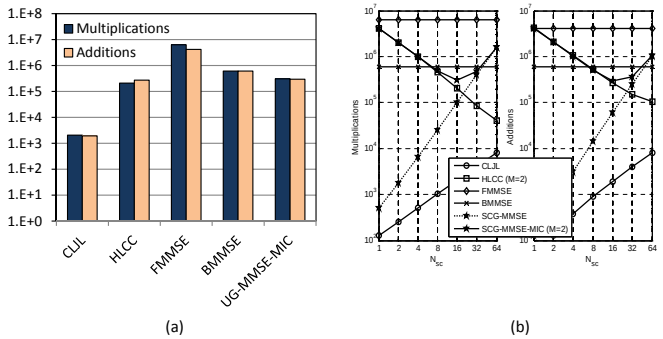

Fig. 3. Complexity comparison (a) Complexity comparison for the UG-MMSE-MIC scheme against other existing schemes. (b) Complexity in terms of multiplications and additions against N_{sc} for the SCG-MMSE-MIC against other existing schemes.

TABLE I

THE PSEUDO CODE FOR THE m-TH IC UNIT FOR (A) THE UG-MMSE-MIC SCHEME (B) THE SCG-MMSE-MIC SCHEME..

(a)

1: **for** $k = 1$ to K **do**
2: Initiating $\boldsymbol{s}^{(m)} = \mathbf{0}_N$, where $\mathbf{0}_N$ is the zeros column vector of order N.
3: Mapping $(\hat{\boldsymbol{s}}_1^{(m-1)}, ..., \hat{\boldsymbol{s}}_{k-1}^{(m-1)}, \hat{\boldsymbol{s}}_{k+1}^{(m-1)}, ..., \hat{\boldsymbol{s}}_K^{(m-1)})$ to $\boldsymbol{s}^{(m)}$;
4: $\boldsymbol{Y}^{(m)} = \boldsymbol{Y} - \boldsymbol{\Pi}\boldsymbol{s}^{(m)}$;
5: $\boldsymbol{Y}_k^{(m)} = \boldsymbol{Y}^{(m)}(\boldsymbol{\mathcal{I}}_k)$;
6: $\boldsymbol{z}_k^{(m)} = \boldsymbol{W}_k^H \boldsymbol{Y}_k^{(m)}$;
7: $\hat{\boldsymbol{s}}_k^{(m)} = \hat{\boldsymbol{s}}_k^{(m-1)} = \mathrm{Restore}(\boldsymbol{z}_k)$;
8: **end for**

(b)

1: **for** $g = 1$ to G **do**
2: Initiating $\boldsymbol{s}^{(m)} = \mathbf{0}_N$, where $\mathbf{0}_N$ is the zeros column vector of order N.
3: Mapping $(\hat{\boldsymbol{s}}_1^{(m-1)}, ..., \hat{\boldsymbol{s}}_{g-1}^{(m-1)}, \hat{\boldsymbol{s}}_{g+1}^{(m-1)}, ..., \hat{\boldsymbol{s}}_G^{(m-1)})$ to $\boldsymbol{s}^{(m)}$;
4: $\boldsymbol{Y}^{(m)} = \boldsymbol{Y} - \boldsymbol{\Pi}\boldsymbol{s}^{(m)}$;
5: $\boldsymbol{Y}_g^{(m)} = \boldsymbol{Y}^{(m)}(\boldsymbol{\mathcal{I}}_g)$;
6: $\boldsymbol{z}_g^{(m)} = \boldsymbol{W}_g^H \boldsymbol{Y}_g^{(m)}$;
7: $\hat{\boldsymbol{s}}_g^{(m)} = \hat{\boldsymbol{s}}_g^{(m-1)} = \mathrm{Restore}(\boldsymbol{z}_k)$;
8: **end for**

TABLE II

COMPUTATIONAL COMPLEXITY OF ALGORITHMS.

Algorithm	Number of operations per block	
	Multiplications	Additions
CLJL [16]	KN_c^2	$KN_c^2 - KN_c$
HLCC [10]	$MKN^2 + (K + 2MK)N_c^2 - 2MKN_cN$	$MKN^2 + (K + 2MK)N_c^2 - (K + MK)N_c$
FMMSE	$3N^3 + N^2 + N$	$2N^3 - 2N^2 + N$
BMMSE [18]	$5N\tau^2 + 9N\tau + 3N$	$5N\tau^2 + 8N\tau + 2N$
UG-MMSE	$3KN_c^3 + KN_c^2 + N_c$	$2KN_c^3 - 2KN_c^2 + KN_c$
UG IC Unit	$KN^2 - 2KNN_c + 2KN_c^2$	$KN^2 - KNN_c + KN_c^2 - KN_c$
UG-MMSE-MIC	$MKN^2 - 2MKNN_c + 3KN_c^3 + (K + 2MK)N_c^2$	$MKN^2 - MKNN_c + 2KN_c^3 + (MK - 2K)N_c^2 + (K - MK)N_c$
SCG-MMSE	$3GN_{sc}^3 + GN_{sc}^2 + N_{sc}$,	$2GN_{sc}^3 - 2GN_{sc}^2 + GN_{sc}$,
SCG IC Unit	$GN^2 - 2GNN_{sc} + 2GN_{sc}^2$	$GN^2 - GNN_{sc} + GN_{sc}^2 - GN_{sc}$
SCG-MMSE-MIC	$MGN^2 - 2MGNN_{sc} + 3GN_{sc}^3 + (G + 2MG)N_{sc}^2$	$MGN^2 - MGNN_{sc} + 2GN_{sc}^3 + (MG - 2G)N_{sc}^2 + (G - MG)N_{sc}$

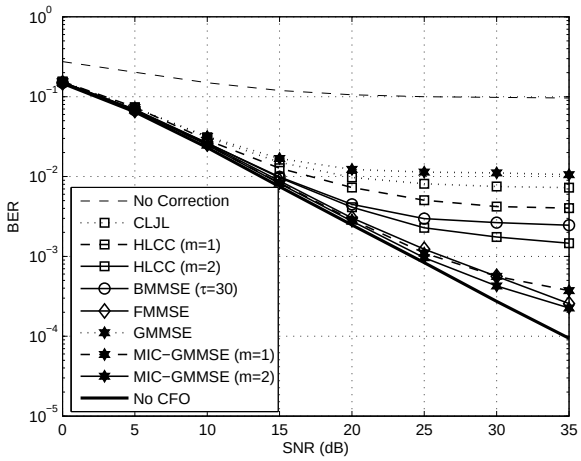

Fig. 4. BER against SNR performance comparison of the UG-MMSE-MIC scheme and other existing schemes using the SCAS and the BPSK signal.

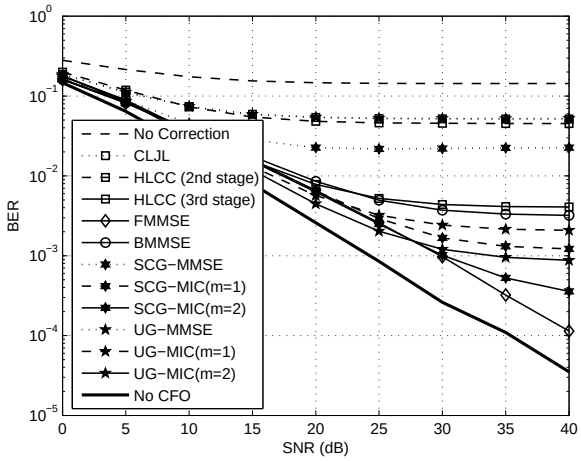

Fig. 5. BER against SNR performance comparison of the UG-MMSE-MIC scheme, the SCG-MMSE-MIC scheme and other existing schemes using the GCAS and the BPSK signal. For the SCG-MMSE-MIC scheme, N_{sc} is set to 16.

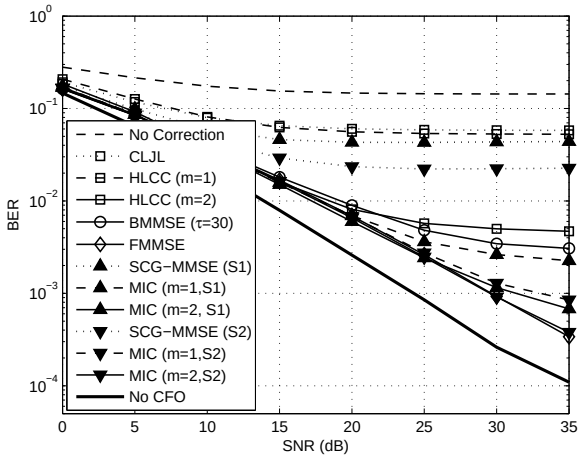

Fig. 6. BER against SNR performance comparison of the SCG-MMSE-MIC scheme and other existing schemes for the GCAS and the BPSK signal in the second scenario, with $k = 8, N_c = 16$. S1 stands for the first setting with $N_{sc} = 4$; S2 stands for the second setting with $N_{sc} = 16$.

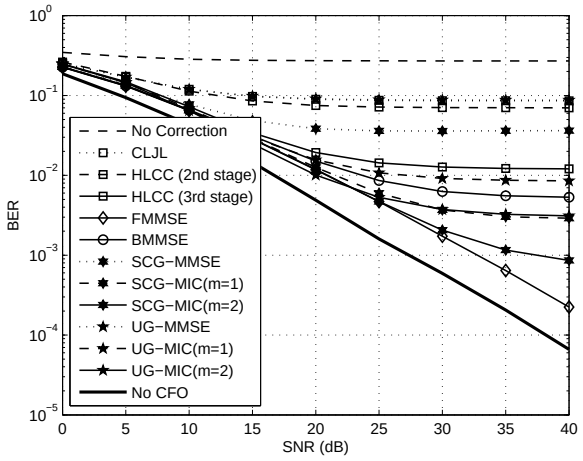

Fig. 7. BER against SNR performance comparison of the UG-MMSE-MIC scheme, the SCG-MMSE-MIC scheme and other existing schemes using the GCAS and the QPSK signal.

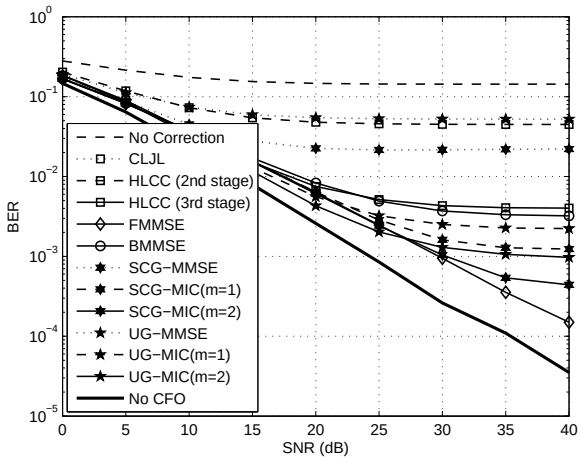

Fig. 8. BER against SNR performance comparison of the UG-MMSE-MIC scheme, the SCG-MMSE-MIC scheme and other existing schemes using the GCAS and the BPSK signal, considering CFO estimation errors.

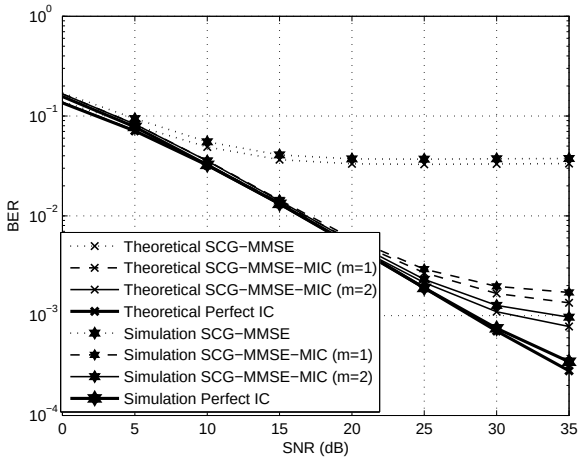

Fig. 9. BER against SNR performance comparison between the theoretical results and the simulation results in a demonstration scenario with N=8 subcarriers, K=4 users, channel order N_h=4, N_{sc}=4 subcarriers in each group and G=2 groups.